Chinese Physics Letters **40**, 047303 (2023) **Express Letter**

Coupled Ferroelectricity and Correlated States in a Twisted Quadrilayer MoS_2 Moiré Superlattice

Fanfan Wu(吴帆帆)[1,2], Lu Li(李璐)[1,2], Qiaoling Xu(徐巧玲)[3,4], Le Liu(刘乐)[1,2], Yalong Yuan(袁亚龙)[1,2], Jiaojiao Zhao(赵交交)[1,2], Zhiheng Huang(黄智恒)[1,2], Xiaozhou Zan(昝晓洲)[1,2], Kenji Watanabe[5], Takashi Taniguchi[6], Dongxia Shi(时东霞)[1,2,3], Lede Xian(冼乐德)[3], Wei Yang(杨威)[1,2,3], Luojun Du(杜罗军)[1,2*], and Guangyu Zhang(张广宇)[1,2,3*]

[1]*Beijing National Laboratory for Condensed Matter Physics, and Institute of Physics, Chinese Academy of Sciences, Beijing 100190, China*
[2]*School of Physical Sciences, University of Chinese Academy of Sciences, Beijing 100049, China*
[3]*Songshan Lake Materials Laboratory, Dongguan 523808, China*
[4]*College of Physics and Electronic Engineering, Center for Computational Sciences, Sichuan Normal University, Chengdu 610068, China*
[5]*Research Center for Functional Materials, National Institute for Materials Science, 1-1 Namiki, Tsukuba 305-0044, Japan*
[6]*International Center for Materials Nanoarchitectonics, National Institute for Materials Science, 1-1 Namiki, Tsukuba 305-0044, Japan*

(Received 27 February 2023; accepted manuscript online 17 March 2023)

Moiré superlattices have emerged as a highly controllable quantum platform for exploration of various fascinating phenomena, such as Mott insulator states, ferroelectric order, unconventional superconductivity and orbital ferromagnetism. Although remarkable progress has been achieved, current research in moiré physics has mainly focused on the single species properties, while the coupling between distinct moiré quantum phenomena remains elusive. Here we demonstrate, for the first time, the strong coupling between ferroelectricity and correlated states in a twisted quadrilayer MoS_2 moiré superlattice, where the twist angles are controlled in sequence to be $\sim 57^\circ$, $\sim 0^\circ$, and $\sim -57^\circ$. Correlated insulator states are unambiguously established at moiré band filling factors $v = 1$, 2, 3 of twisted quadrilayer MoS_2. Remarkably, ferroelectric order can occur at correlated insulator states and disappears quickly as the moiré band filling deviates from the integer fillings, providing smoking gun evidences of the coupling between ferroelectricity and correlated states. Our results demonstrate the coupling between different moiré quantum properties and will hold great promise for new moiré physics and applications.

DOI: 10.1088/0256-307X/40/4/047303

Two-dimensional (2D) layered materials, because of the weak coupling between adjacent layers, offer a plethora of opportunities to construct van der Waals (vdW) heterostructures without the constraint of lattice matching and processing compatibility in conventional heterostructures.[1–4] It is well known that vdW heterostructures constitute a wide range of new quantum metamaterials with fascinating electrical, optical, magnetic and topological properties, as they are defined not only by the best characteristics of constituent 2D layers, but also by the interlayer quantum coupling.[1,2] Remarkably, a geometrical moiré superlattice can be formed in vdW heterostructures when the misalignment between the constituent 2D atomic layers is small, e.g., two identical lattices with a tiny twist angle or two dissimilar materials with a slight lattice mismatch.[5,6] Moiré superlattices introduce a new length scale much larger than the periodicity of the constituent layers, endowing a highly controllable system to engineer the electronic band structure for a plethora of emergent quantum phenomena.[5,7] For example, the formation of flat electronic bands in strong-coupling moiré superlattices can favor on-site Coulomb repulsion interaction over the kinetic lattice hopping, giving rise to a rich phase diagram of strongly correlated and topological states,[5] including but not limited to correlated insulator states,[8–10] orbital magnetism,[11–14] Wigner crystal states,[15,16] ferroelectricity,[17–19] and unconventional superconductivity.[20–22] Meanwhile, a host of exotic photonic and optoelectronic phenomena can emerge when the moiré superlattice is coupled with light, such as moiré excitons,[23,24] ultra-low-threshold broadband moiré laser,[25] tunable quantum light sources,[26] and intelligent infrared sensing.[27] Although notable progress has been witnessed in moiré physics with an unprecedented speed, current research has mainly focused on the single species prop-

*Corresponding authors. Email: luojun.du@iphy.ac.cn; gyzhang@iphy.ac.cn

erties, while the coupling between distinct moiré quantum phenomena has not yet been explored.

In this Letter, we demonstrate the strong coupling between ferroelectric polarization and correlated states in a twisted quadrilayer MoS_2 moiré superlattice, where the twist angles are controlled to be $\sim 57°$ ($-57°$) between the first (third) and second (fourth) layers, and $\sim 0°$ between the second and third layers. Correlated insulator insulating states are unambiguously established at moiré band filling factors $\nu = 1$, 2, 3, corresponding to one, two, and three electrons per moiré superlattice site. Remarkably, appreciable ferroelectric polarization can occur at correlated insulator states and decreases rapidly as the moiré band filling deviates from the integer fillings, evidencing the intrinsic coupling between ferroelectricity and correlated electronic states.

Results.—Stacking Effects on Moiré Physics. Figures 1(a) and 1(b) show the schematic diagrams of AB-stacked and AA-stacked MoS_2 homobilayer moiré superlattices, respectively. Long-period moiré patterns can be clearly seen in both cases. For AA stacking, there are three high-symmetry sites in the superlattice: (i) the R_X^M site, in which the Mo atom lays directly on top of the S atoms; (ii) the R_M^X site, the inverse of the R_X^M site; (iii) the R_M^M site with Mo atoms in one layer directly on top of Mo atoms in the other layer. The high-symmetry sites in AB stacking are different, including the H_X^M site (the stacking structure of natural bilayer MoS_2) and the H_M^M and H_X^X sites.[7,26] Figures 1(c) and 1(d) present the electronic band structures of commensurate 56.85° and 3.15° twisted bilayer MoS_2, respectively, by density functional theory (DFT) calculations. Clearly, multiple energy-separated ultra-flat moiré minibands with a band width less than 10 meV can emerge at the conduction band edge of 56.85° twisted bilayer MoS_2. By contrast, the energy bands at the conduction band edge of 3.15° twisted bilayer MoS_2 show considerable dispersion. This indicates that stacking order plays a paramount role in tailoring the electronic band structure and electron correlations of twisted bilayer MoS_2 moiré superlattices, in agreement with the recent theoretical calculation.[28,29]

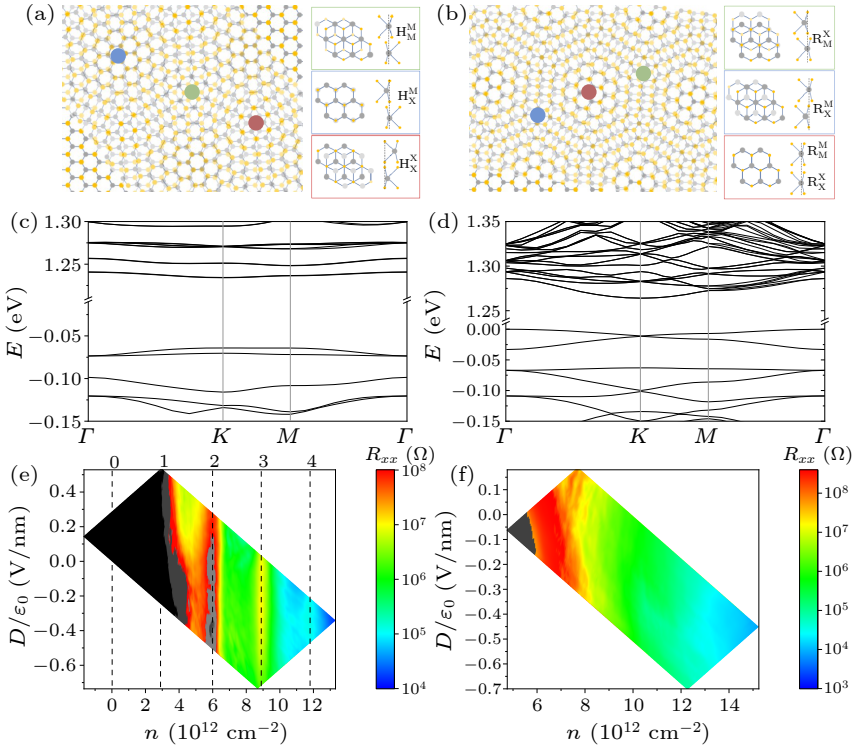

Fig. 1. Stacking effects on moiré physics. [(a), (b)] The atomic configuration of AB-stacked (a) and AA-stacked (b) MoS_2 homobilayer moiré superlattices. Right panels are the corresponding close-ups of high-symmetry points of the moiré unit cell. [(c), (d)] The electronic band structure of 56.85° (c) and 3.15° (d) twisted bilayer MoS_2 in the first mini-Brillouin zone. [(e), (f)] Four-terminal resistance at 10 K as functions of carrier densities and displacement fields of AB-stacked (e) and AA-stacked (f) bilayer MoS_2 moiré superlattices.

To uncover the stacking effects on moiré physics, we fabricate hexagonal boron nitride (h-BN) encapsulated, dual-gated twisted bilayer MoS_2 moiré superlattice devices of both AB stacking (twist angle is controlled to be at $\sim 57°$) and AA stacking (twist angle is controlled to be at $\sim 3°$) utilizing the 'cut and stack' technique.[10] It is noteworthy that monolayer MoS_2 single crystal samples grown by vdW epitaxial tech-

nique are adopted, which show better electronic qualities than the exfoliated ones.[30] The dual-gate configuration enables us to independently tune the carrier density $n = (C_\mathrm{b}V_\mathrm{b} + C_\mathrm{t}V_\mathrm{t})/e$ and out-of-plane displacement field $D = (C_\mathrm{b}V_\mathrm{b} - C_\mathrm{t}V_\mathrm{t})/2$, where e is the elementary charge, C_b (V_b) and C_t (V_t) are the geometrical capacitances per area (applied voltages) for bottom and top gates, respectively.[10] Figures 1(e) and 1(f) show the 2D color plot of four-terminal longitudinal resistance at 10 K as functions of electron densities and out-of-plane displacement fields for AB-stacked and AA-stacked bilayer MoS_2 moiré superlattices, respectively. For twisted bilayer MoS_2 of AB stacking, four strong resistance peaks are clearly observed at $n = n_0$, $2n_0$, $3n_0$, and $4n_0$, coinciding with 1, 2, 3, and 4 electrons per moiré superlattice site (that is, moiré band filling factors $v = 1$, 2, 3, 4). Here, $n_0 = 8[\sin(\frac{60^\circ-\theta}{2})]^2/[\sqrt{3}a^2] = 2.9 \times 10^{12}\,\mathrm{cm}^{-2}$ corresponds to the moiré density that is one electron per superlattice site, where $a = 0.315$ nm denotes the MoS_2 lattice constant and θ is the twist angle.[31] Note that the diverging resistance peaks at $n = 0$ mark the intrinsic band edge of MoS_2. The appearance of insulating states at $v = 1$, 2, 3, 4 defies the description by single-particle band structure paradigm and unequivocally demonstrates the moiré-induced flat conduction bands in twisted bilayer MoS_2 of AB stacking. In marked contrast, twisted bilayer MoS_2 of AA stacking does not show any correlated insulator states [Fig. 1(f)], in good harmony with the theoretical calculations without flat conduction bands [Fig. 1(d)]. It is worth noting that despite the lack of correlated states, recent advances have shown that AA-stacked bilayer MoS_2 moiré superlattices can show unique ferroelectric polarization.[17,18]

Coexistence of Correlated States and Ferroelectricity. Considering that AB-stacked and AA-stacked MoS_2 homobilayer moiré superlattices show different advantages (i.e., correlated insulator states in AB stacking and ferroelectricity in AA stacking), a multilayer MoS_2 moiré superlattice containing these two stacking orders may enable us to meet unprecedented opportunities to realize the coexistence of correlated states and ferroelectricity order. Figure 2(a) schematically shows the typical structure of h-BN encapsulated, dual-gated twisted quadrilayer MoS_2 moiré superlattice devices, with gold (silicon) as the top (bottom) gate. The twist angles between two adjacent layers are controlled in sequence to be $\sim 57^\circ$ (i.e., AB stacking), $\sim 0^\circ$ (i.e., AA stacking), and $\sim -57^\circ$ (i.e., AB stacking). Figure 2(b) shows the optical microscope image of the twisted quadrilayer MoS_2 before h-BN encapsulation, with each layer outlined by colored lines. The optical image of final device with multiple electrodes is shown in Fig. 2(c). Note that few-layer graphene is used as contact to ensure a good contact for transport measurements.[32,33]

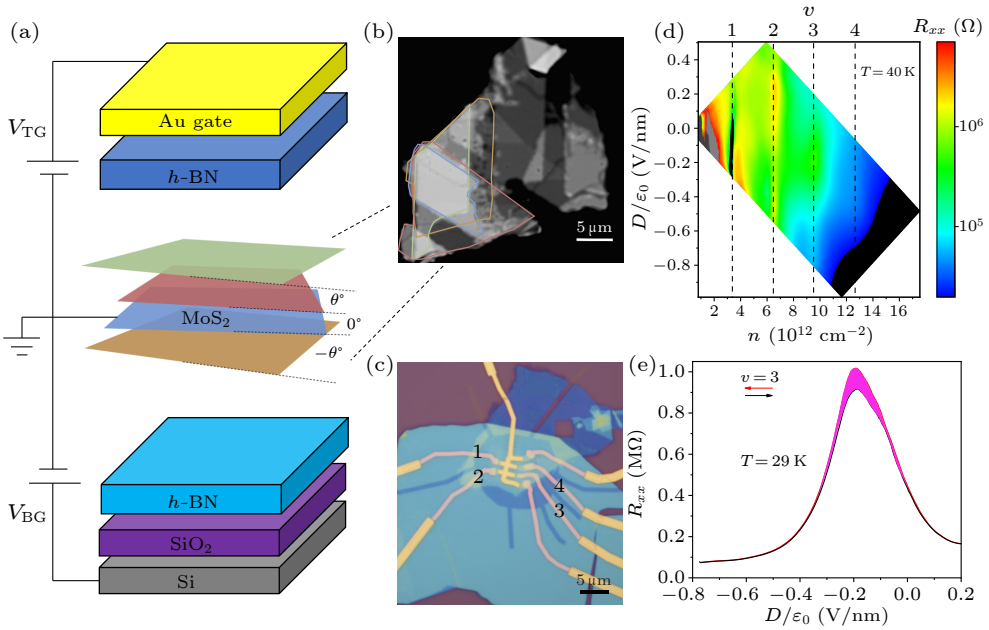

Fig. 2. The coexistence of correlated insulating states and ferroelectricity in a twisted quadrilayer MoS_2 moiré superlattice. (a) Schematic geometry of the h-BN encapsulated, dual-gated twisted quadrilayer MoS_2 moiré superlattice device. (b) Optical microscope image of the twisted quadrilayer MoS_2 before h-BN encapsulation. (c) Optical image of the final device with multiple electrodes. Contacts 3 and 4 are used for current injection and excitation, contacts 1 and 2 are served as signal detection. (d) Four-terminal resistance as functions of displacement fields and carrier densities. The insulating states are marked by dashed lines. (e) Resistance hysteresis at moiré band filling factor $v = 3$.

Figure 2(d) plots the 2D color map of the four-terminal resistance as functions of carrier densities and displacement fields at 40 K. In close analogy to the twisted bilayer MoS_2 of AB stacking, the twisted quadrilayer MoS_2 moiré superlattice clearly shows strong resistance peaks at moiré band filling factors $v = 1, 2, 3, 4$. This demonstrates the moiré-induced flat conduction bands and the formation of correlated electronic states in twisted quadrilayer MoS_2. Figure 2(e) presents the resistance against the displacement fields at moiré band filling factor $v = 3$. Importantly, the resistance of $v = 3$ shows a significant hysteresis window (outlined by red region), when the displacement field is swept back and forth between -0.8 V/nm and 0.2 V/nm. Such resistance hysteresis associated with the scan direction of displacement field suggests the possibility of ferroelectric order in twisted quadrilayer MoS_2 moiré superlattice.[34,35] Additionally, the resistance hysteresis is independent of the scan rate, and the resistance lines are almost overlapped without hysteresis when the displacement field is scanned along the same direction four times (see the Supplementary Information). This largely precludes the potential measurement artifacts (e.g., electronic circuits) and rules out the influence of external disturbances on resistance hysteresis. When scanning carrier density back and forth at a constant displacement field, the resistance hysteresis is also nearly zero (see the Supplementary Information). As a consequence, the appearance of considerable resistance hysteresis associated with the scan direction of displacement field should be indeed from the ferroelectric polarization. In other words, ferroelectric polarization and correlated insulator states can coexist in twisted quadrilayer MoS_2 moiré superlattice containing both the AA and AB stacking orders. By contrast, for a 57.5° twisted bilayer MoS_2 moiré superlattice, although correlated states at moiré band filling factors $v = 1, 2, 3$ can be clearly observed, the resistance lines are almost overlapped without hysteresis when scanned along different directions. This strongly indicates the absence of ferroelectric polarization in AB-stacked MoS_2 homobilayer moiré superlattices (also see the Supplementary Information).

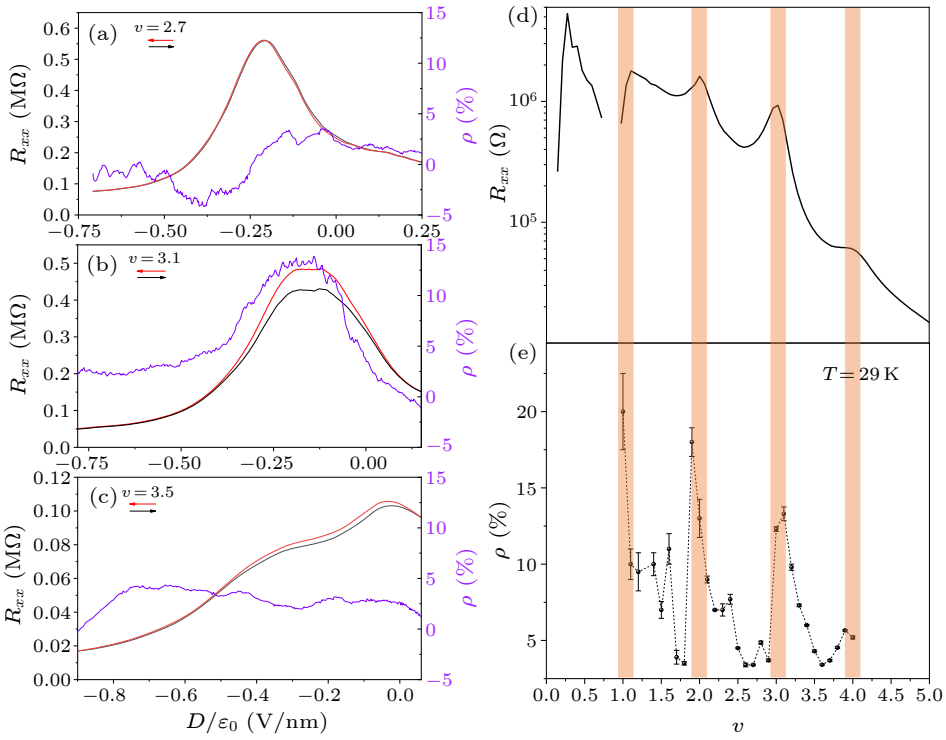

Fig. 3. Coupled insulating states and ferroelectricity in twisted quadrilayer MoS_2 moiré superlattice. (a)–(c) Ferroelectric hysteresis and the calculated ferroelectric polarization $\rho = (\overleftarrow{R} - \overrightarrow{R})/\overrightarrow{R}$ at $v = 2.7$ (a), $v = 3.1$ (b), and $v = 3.5$ (c). The temperature is 29 K. [(d), (e)] Four-terminal resistance (d) and ferroelectric polarization ρ (e) versus moiré band filling factors.

The Coupling between Correlated States and Ferroelectricity. Having identified the coexistence of ferroelectric polarization and correlated insulator states, now a natural question arises: Can ferroelectricity and correlated states be coupled with each other? To demystify this, we study the ferroelectric polarization against the moiré band filling factors. Figures 3(a), 3(b), and 3(c) show the displacement-field-dependent

resistance at moiré band filling factors of $v = 2.7$, 3.1, and 3.5, respectively. Clearly, the resistance hysteresis depends strongly on the moiré band filling factors. We quantify the magnitude of ferroelectric polarization by $\rho = (\overleftarrow{R} - \overrightarrow{R})/\overrightarrow{R}$, where $\overleftarrow{R}$ ($\overrightarrow{R}$) denotes the resistance value when scanning the displacement field from positive (negative) to negative (positive). Figures 3(d) and 3(e) show the four-terminal resistance and the magnitude of ferroelectric polarization ρ, respectively, versus moiré band filling factors at a temperature of 29 K. Remarkably, the ferroelectric polarization ρ shows the maximum values near moiré band filling factors $v = 1$, 2, 3, 4 (i.e., correlated insulator states), and decreases sharply as the filling factor deviates from integer fillings. This strongly indicates that ferroelectricity and correlated states are coupled with each other in twisted quadrilayer MoS_2 moiré superlattice. We envision that the coupling between different moiré quantum properties will stimulate great interest in theory and experiment, and hold great promise for new moiré physics and applications.

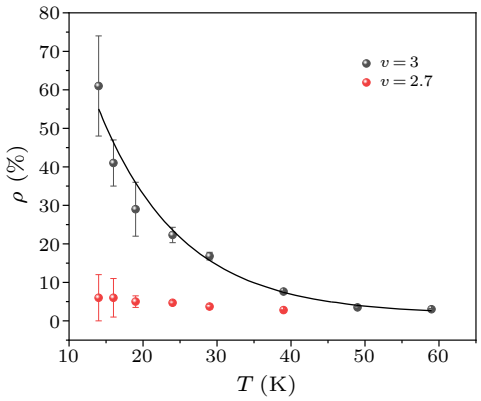

Fig. 4. Temperature dependence of ferroelectric polarization at $v = 3$ (black) and $v = 2.7$ (red). The black solid line represents the exponential decay fit $\rho \propto e^{-\alpha/T}$.

Temperature-Dependent Ferroelectric Polarization. Considering that correlated electronic states are sensitive to temperature, the ferroelectric polarization in principle would also strongly depend on temperature. Figure 4 presents the magnitude of ferroelectric polarization ρ at the moiré band filling factors $v = 3$ and $v = 2.7$ as a function of temperatures. Please see the temperature dependent-ferroelectric polarization ρ at $v = 1.2$ in the Supplementary Information. For $v = 2.7$, the ferroelectric polarization ρ can always be ignored in the temperature range we investigated (14 K–60 K). By contrast, ferroelectric polarization ρ at $v = 3$ can reach $\sim$60% at 14 K and decreases with increasing temperature. The ferroelectric polarization ρ at $v = 3$ can be fitted well by an exponential decay function $\rho \propto e^{-\alpha/T}$ (the black solid line). This indicates that ferroelectric polarization ρ decreases exponentially with increasing temperature, bearing striking resemblance to temperature-driven evolution of correlated insulator states.[31]

In conclusion, we demonstrate the coupling between ferroelectric polarization and correlated states in a twisted quadrilayer MoS_2 moiré superlattice, containing both the AA and AB stacking orders. Correlated insulator states are unambiguously established at moiré band filling factors $v = 1$, 2, 3 of twisted quadrilayer MoS_2. Furthermore, ferroelectric polarization shows the maximum values near correlated insulator states and decreases quickly as the moiré band filling deviates from the integer fillings, evidencing of the coupling between ferroelectricity and correlated states. Our results demonstrate the coupling between different moiré quantum properties and will hold great promise for not only the interweaving of different research directions but also new physics and applications.

Acknowledgements. This work was supported by the Key-Area Research and Development Program of Guangdong Province, China (Grant No. 2020B0101340001), the National Key Research and Development Program of China (Grant Nos. 2021YFA1202900 and 2020YFA0309600), the National Science Foundation of China (Grant Nos. 61888102, 11834017, 1207441, and 12274447), and the Strategic Priority Research Program of CAS (Grant Nos. XDB30000000 and XDB33000000). K.W. and T.T. acknowledge the supports from the Elemental Strategy Initiative conducted by the MEXT, Japan (Grant No. JPMXP0112101001), JSPS KAKENHI (Grant Nos. 19H05790, 20H00354, and 21H05233) and A3 Foresight by JSPS.

References

[1] Novoselov K S, Mishchenko A, Carvalho A, and Castro N A H 2016 *Science* **353** aac9439
[2] Jin C H, Ma E Y, Karni O, Regan E C, Wang F, and Heinz T F 2018 *Nat. Nanotechnol.* **13** 994
[3] Liu Y, Weiss N O, Duan X, Cheng H C, Huang Y, and Duan X F 2016 *Nat. Rev. Mater.* **1** 16042
[4] Du L J, Hasan T, Castellanos-Gomez A, Liu G B, Yao Y G, Lau C N, and Sun Z P 2021 *Nat. Rev. Phys.* **3** 193
[5] Andrei E Y, Efetov D K, Jarillo-Herrero P, MacDonald A H, Mak K F, Senthil T, Tutuc E, Yazdani A, and Young A F 2021 *Nat. Rev. Mater.* **6** 201
[6] Chu Y B, Liu L, Yuan Y L, Shen C, Yang R, Shi D X, Yang W, and Zhang G Y 2020 *Chin. Phys. B* **29** 128104
[7] Mak K F and Shan J 2022 *Nat. Nanotechnol.* **17** 686
[8] Cao Y, Fatemi V, Demir A, Fang S, Tomarken S L, Luo J Y, Sanchez-Yamagishi J D, Watanabe K, Taniguchi T, Kaxiras E, Ashoori R C, and Jarillo-Herrero P 2018 *Nature* **556** 80
[9] Chen G R, Jiang L L, Wu S, Lyu B, Li H Y, Chittari B L, Watanabe K, Taniguchi T, Shi Z W, Jung J, Zhang Y B, and Wang F 2019 *Nat. Phys.* **15** 237
[10] Shen C, Chu Y B, Wu Q S, Li N, Wang S P, Zhao Y C, Tang J, Liu J Y, Tian J P, Watanabe K, Taniguchi T,

Yang R, Meng Z Y, Shi D X, Yazyev O V, and Zhang G Y 2020 *Nat. Phys.* **16** 520

[11] Sharpe A L, Fox E J, Barnard A W, Finney J, Watanabe K, Taniguchi T, Kastner M A, and Goldhaber-Gordon D 2019 *Science* **365** 605

[12] Chen G R, Sharpe A L, Fox E J, Zhang Y H, Wang S X, Jiang L L, Lyu B, Li H Y, Watanabe K, Taniguchi T, Shi Z W, Senthil T, Goldhaber-Gordon D, Zhang Y B, and Wang F 2020 *Nature* **579** 56

[13] Shen C, Ying J H, Liu L, Liu J P, Li N, Wang S P, Tang J, Zhao Y C, Chu Y B, Watanabe K, Taniguchi T, Yang R, Shi D X, Qu F M, Lu L, Yang W, and Zhang G Y 2021 *Chin. Phys. Lett.* **38** 047301

[14] Wu S, Zhang Z Y, Watanabe K, Taniguchi T, and Andrei E Y 2021 *Nat. Mater.* **20** 488

[15] Regan E C, Wang D Q, Jin C H, Bakti U M I, Gao B N, Wei X, Zhao S H, Zhao W Y, Zhang Z C, Yumigeta K, Blei M, Carlström J D, Watanabe K, Taniguchi T, Tongay S, Crommie M, Zettl A, and Wang F 2020 *Nature* **579** 359

[16] Xu Y, Liu S, Rhodes D A, Watanabe K, Taniguchi T, Hone J, Elser V, Mak K F, and Shan J 2020 *Nature* **587** 214

[17] Wang X R, Yasuda K, Zhang Y, Liu S, Watanabe K, Taniguchi T, Hone J, Fu L, and Jarillo-Herrero P 2022 *Nat. Nanotechnol.* **17** 367

[18] Weston A, Castanon E G, Enaldiev V, Ferreira F, Bhattacharjee S, Xu S G, Corte-Leon H, Wu Z F, Clark N, Summerfield A, Hashimoto T, Gao Y Z, Wang W D, Hamer M, Read H, Fumagalli L, Kretinin A V, Haigh S J, Kazakova O, Geim A K, Fal'ko V I, and Gorbachev R 2022 *Nat. Nanotechnol.* **17** 390

[19] Zheng Z R, Ma Q, Bi Z, de la B S, Liu M H, Mao N N, Zhang Y, Kiper N, Watanabe K, Taniguchi T, Kong J, Tisdale W A, Ashoori R, Gedik N, Fu L, Xu S Y, and Jarillo-Herrero P 2020 *Nature* **588** 71

[20] Cao Y, Fatemi V, Fang S, Watanabe K, Taniguchi T, Kaxiras E, and Jarillo-Herrero P 2018 *Nature* **556** 43

[21] Chen G R, Sharpe A L, Gallagher P, Rosen I T, Fox E J, Jiang L L, Lyu B, Li H Y, Watanabe K, Taniguchi T, Jung J, Shi Z W, Goldhaber-Gordon D, Zhang Y B, and Wang F 2019 *Nature* **572** 215

[22] Lu X B, Stepanov P, Yang W, Xie M, Aamir M A, Das I, Urgell C, Watanabe K, Taniguchi T, Zhang G Y, Bachtold A, MacDonald A H, and Efetov D K 2019 *Nature* **574** 653

[23] Regan E C, Wang D Q, Paik E Y, Zeng Y X, Zhang L, Zhu J H, MacDonald A H, Deng H, and Wang F 2022 *Nat. Rev. Mater.* **7** 778

[24] Seyler K L, Rivera P, Yu H Y, Wilson N P, Ray E L, Mandrus D G, Yan J Q, Yao W, and Xu X D 2019 *Nature* **567** 66

[25] Lin Q, Fang H, Liu Y, Zhang Y, Fischer M, Li J, Hagel J, Brem S, Malic E, Stenger N, Sun Z, Wubs M, and Xiao S 2023 arXiv:2302.01266 [physcis.optics]

[26] Yu H Y, Liu G B, Tang J J, Xu X D, and Yao W 2017 *Sci. Adv.* **3** e1701696

[27] Ma C, Yuan S F, Cheung P, Watanabe K, Taniguchi T, Zhang F, and Xia F N 2022 *Nature* **604** 266

[28] Xian L D, Claassen M, Kiese D, Scherer M M, Trebst S, Kennes D M, and Rubio A 2021 *Nat. Commun.* **12** 5644

[29] Naik M H, Kundu S, Maity I, and Jain M 2020 *Phys. Rev. B* **102** 075413

[30] Wang Q Q, Tang J, Li X M, Tian J P, Liang J, Li N, Ji D P, Xian L D, Guo Y T, Li L, Zhang Q H, Chu Y B, Wei Z, Zhao Y C, Du L J, Yu H, Bai X D, Gu L, Liu K H, Yang W, Yang R, Shi D X, and Zhang G Y 2022 *Natl. Sci. Rev.* **9** nwac077

[31] Wang L, Shih E M, Ghiotto A, Xian L D, Rhodes D A, Tan C, Claassen M, Kennes D M, Bai Y S, Kim B, Watanabe K, Taniguchi T, Zhu X R, Hone J, Rubio A, Pasupathy A N, and Dean C R 2020 *Nat. Mater.* **19** 861

[32] Cui X, Lee G H, Kim Y D, Arefe G, Huang P Y, Lee C H, Chenet D A, Zhang X, Wang L, Ye F, Pizzocchero F, Jessen B S, Watanabe K, Taniguchi T, Muller D A, Low T, Kim P, and Hone J 2015 *Nat. Nanotechnol.* **10** 534

[33] Xie L, Liao M Z, Wang S P, Yu H, Du L J, Tang J, Zhao J, Zhang J, Chen P, Lu X B, Wang G L, Xie G B, Yang R, Shi D X, and Zhang G Y 2017 *Adv. Mater.* **29** 1702522

[34] Si M W, Saha A K, Gao S J, Qiu G, Qin J K, Duan Y Q, Jian J, Niu C, Wang H Y, Wu W Z, Gupta S K, and Ye P D 2019 *Nat. Electron.* **2** 580

[35] Guan Z, Hu H, Shen X W, Xiang P H, Zhong N, Chu J H, and Duan C G 2020 *Adv. Electron. Mater.* **6** 1900818

Supplementary information

Coupled ferroelectricity and correlated states in a twisted quadrilayer MoS_2 moiré superlattice

Fanfan Wu[1,2], Lu Li[1,2], Qiaoling Xu[3,4], Le Liu[1,2], Yalong Yuan[1,2], Jiaojiao Zhao[1,2], Zhiheng Huang[1,2], Xiaozhou Zan[1,2], Kenji Watanabe[5], Takashi Taniguchi[6], Dongxia Shi[1,2,3], Lede Xian[3], Wei Yang[1,2,3], Luojun Du[1,2]*, Guangyu Zhang[1,2,3]*

[1]*Beijing National Laboratory for Condensed Matter Physics, Institute of Physics, Chinese Academy of Sciences, Beijing 100190, China*

[2]*School of Physical Sciences, University of Chinese Academy of Sciences, Beijing 100049, China*

[3]*Songshan Lake Materials Laboratory, Dongguan, Guangdong 523808, China*

[4]*College of Physics and Electronic Engineering, Center for Computational Sciences, Sichuan Normal University, Chengdu 610068, China*

[5]*Research Center for Functional Materials, National Institute for Materials Science, 1-1 Namiki, Tsukuba 305-0044, Japan*

[6]*International Center for Materials Nanoarchitectonics, National Institute for Materials Science, 1-1 Namiki, Tsukuba 305-0044, Japan*

Email: luojun.du@iphy.ac.cn; gyzhang@iphy.ac.cn

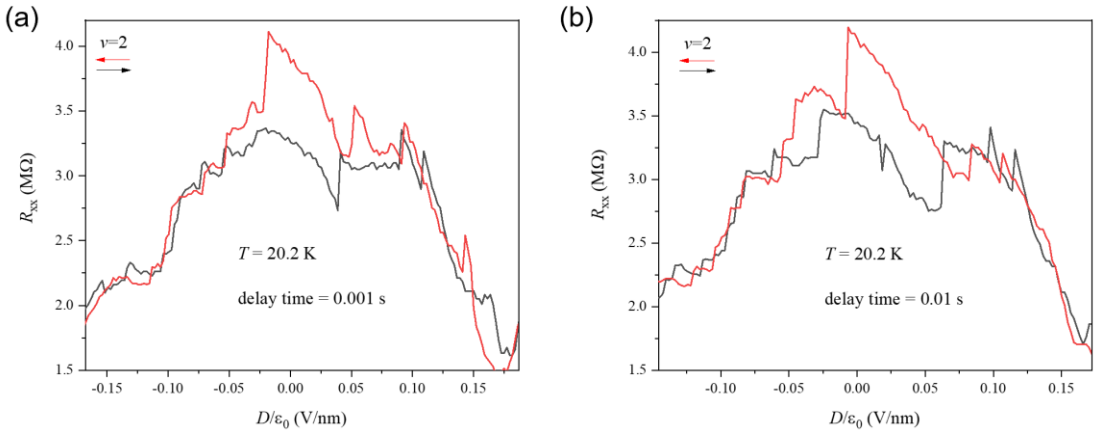

Figure S1. Scanning rate dependence of resistance hysteresis. Scan displacement field back and forth at 20.2 K. Interval of every two points measured is 0.001 s (a) and 0.01 s (b). The measurement time required in (b) is tenfold longer than the time in (a). But the hysteresis window is near same considering a natural decline of build-in electrical field.

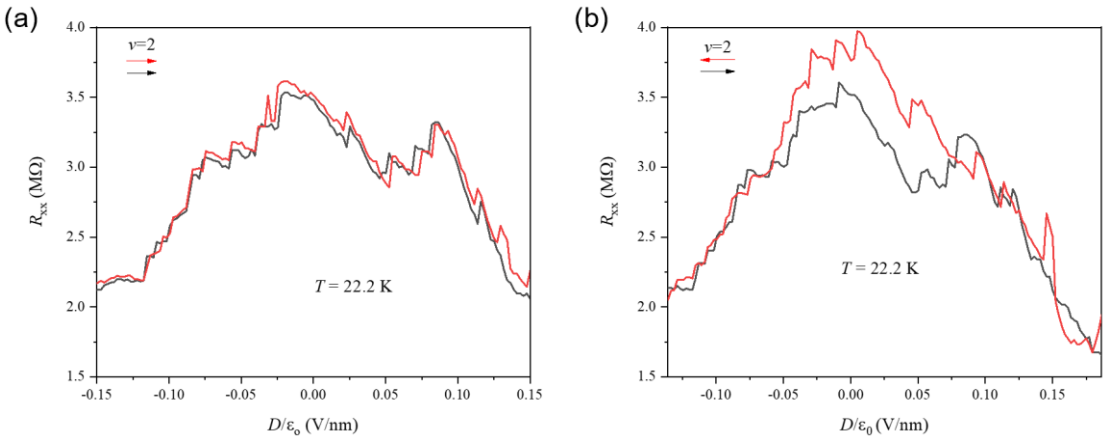

Figure S2. Scanning direction dependence of resistance hysteresis. (a) Two lines are almost overlapped without hysteresis when scanning from -0.15 V/nm to 0.15 V/nm twice at 22.2 K. (b) Two lines show an obvious hysteresis window when scanning firstly from about 0.175 V/nm to -0.125 V/nm and then from about -0.125 V/nm to 0.175 V/nm at 22.2 K.

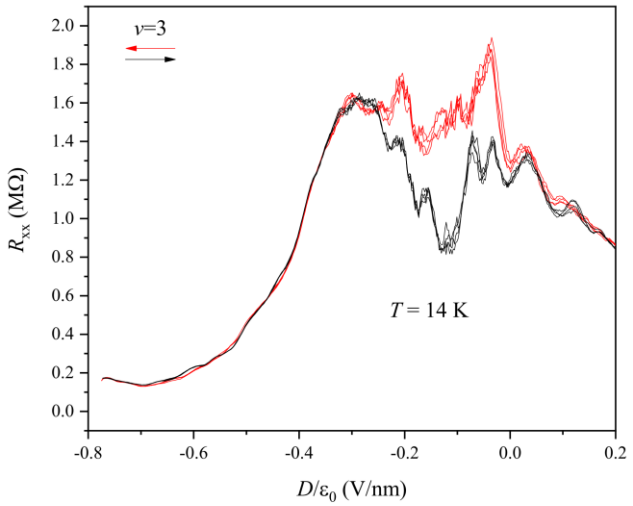

Figure S3. The resistance hysteresis against the scanning directions for ν = 3 at 14 K. For each direction, we repeated the measurements four times. The resistance lines are almost overlapped without hysteresis when scanned in the same direction. By contrast, the resistance lines show an obvious hysteresis window when scanned along different directions.

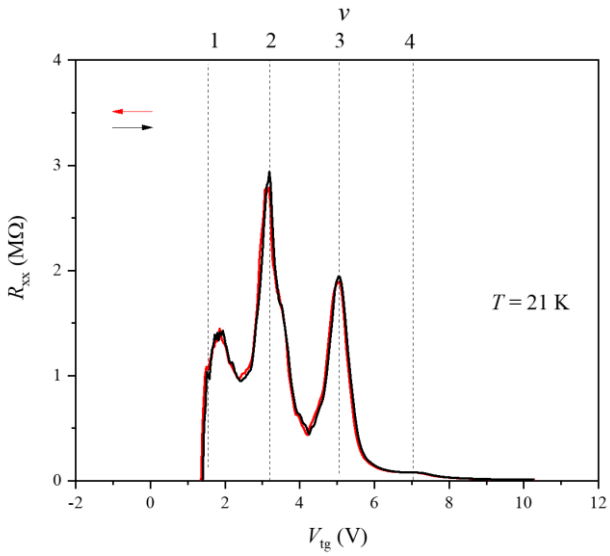

Figure S4. Doping dependent hysteresis at different filling factors. There is no obvious hysteresis when scanning carrier density back and forth at a constant displacement field.

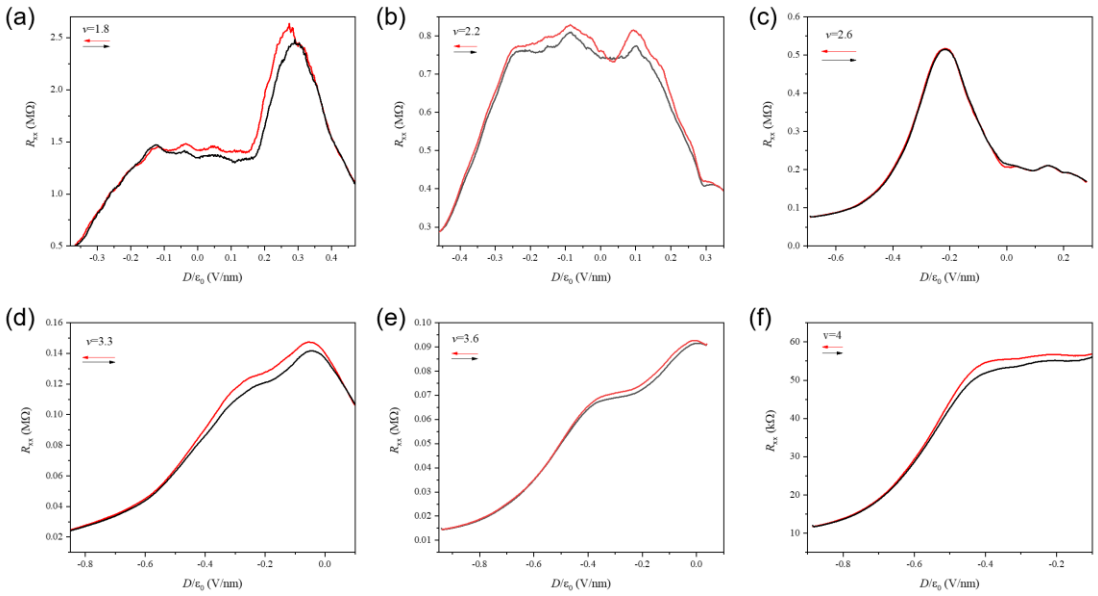

Figure S5. Ferroelectric hysteresis at various filling factors. Universal ferroelectric hysteresis lines are seen at various filling factors in (a)-(f).

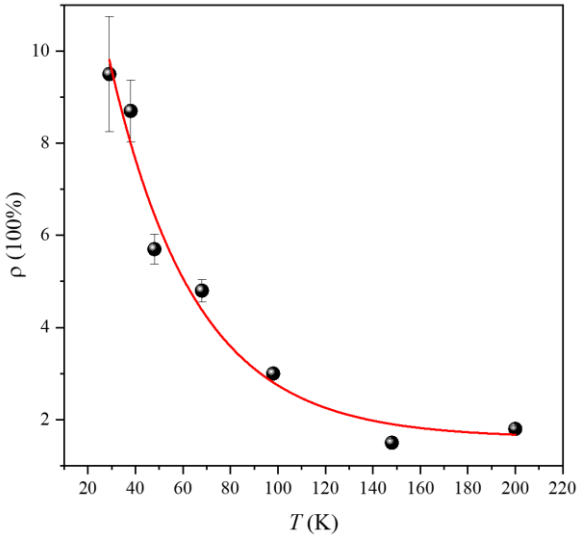

Figure S6. Temperature dependence of ferroelectric polarization at ν = 1.2. The red solid line represents the exponential decay fit $\rho \propto e^{-\alpha/T}$.

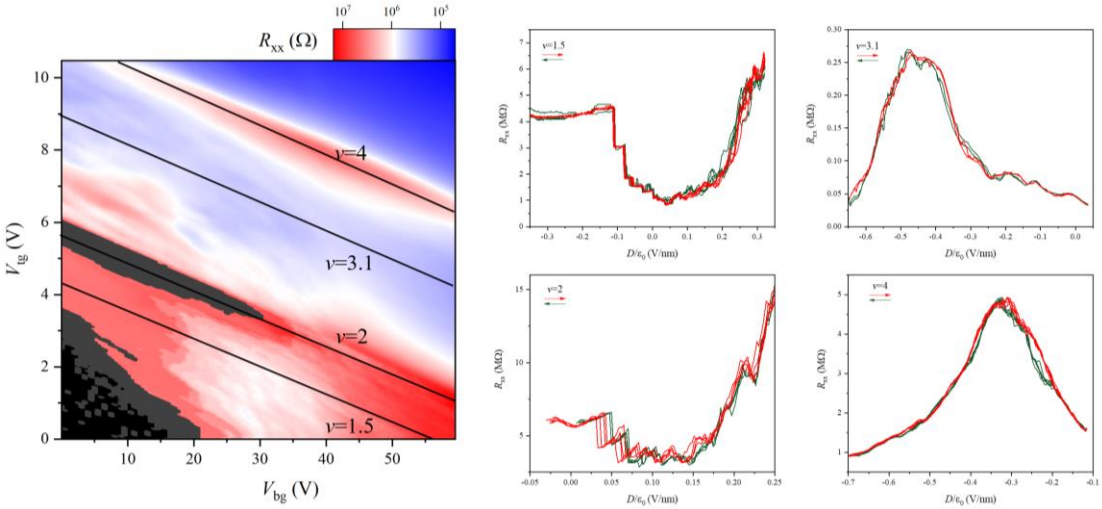

Figure S7. The absence of ferroelectric polarization in 57. 5° twisted bilayer MoS_2. The measured temperature is 12.5 K. Although correlated states at moiré band filling factors ν = 1, 2, 3 can be clearly observed in 57. 5° twisted bilayer MoS_2 moiré superlattice, the resistance lines are almost overlapped without hysteresis when scanned along different directions. This strongly indicates the absence of ferroelectric polarization in 57. 5° twisted bilayer MoS_2.